CONTEXT-DEPENDENT AND DYNAMIC FUNCTIONAL INFLUENCE OF CORTICOTHALAMIC PATHWAYS TO FIRST- AND HIGHER-ORDER VISUAL THALAMUS

Megan A. Kirchgessner[1,2], Alexis D. Franklin[1] & Edward M. Callaway[1,2,3*]

1. Systems Neurobiology Laboratories, Salk Institute for Biological Studies, La Jolla, CA 92037, USA
2. Neurosciences Graduate Program, University of California San Diego, La Jolla, CA 92093, USA
3. Lead Contact

* Correspondence: callaway@salk.edu

Summary

Layer 6 (L6) is the sole purveyor of corticothalamic (CT) feedback to first-order thalamus and also sends projections to higher-order thalamus, yet how it engages the full corticothalamic circuit to contribute to sensory processing in an awake animal remains unknown. We sought to elucidate the functional impact of L6 CT projections from primary visual cortex to first- and higher-order visual thalamic nuclei dLGN and pulvinar using optogenetics and extracellular electrophysiology in awake mice. While sustained L6 CT photostimulation largely suppresses activity in both visual thalamic nuclei, moderate-frequency stimulation powerfully facilitates spiking in dLGN and pulvinar *in vivo*. We show that each stimulation paradigm differentially influences the balance between monosynaptic excitatory and disynaptic inhibitory (via thalamic reticular nucleus) corticothalamic pathways to dLGN and pulvinar. Altogether, our results support a model in which L6 CTs modulate first- and higher-order thalamus through parallel excitatory and inhibitory pathways that are highly dynamic and context-dependent.

Introduction

While the flow of information from thalamus to cortex is widely appreciated as a critical step in sensory processing, the significance of a given cortical area's projection back to thalamus - both to the thalamic source of its input (first-order nuclei) as well as to other "higher-order" thalamic nuclei - is considerably less clear. In the case of first-order nuclei, like the dorsal lateral geniculate nucleus (dLGN) in the visual system, this corticothalamic feedback originates from layer 6. Layer 6 corticothalamic neurons (L6 CTs) have been classically described as providing "modulatory" feedback to dLGN (Sherman and Guillery, 1998) and have been implicated in processes such as response gain (Denman and Contreras, 2015; Olsen et al., 2012; Przybyszewski et al., 2000; Wang et al., 2006, 2018), temporal precision (Andolina et al., 2007; Hasse and Briggs, 2017), spatiotemporal filtering (Andolina et al., 2013; Hasse and Briggs, 2017; Wang et al., 2018), firing mode (Andolina et al., 2013; Mease et al., 2014; Wang et al., 2006), and sensory adaptation (Mease et al., 2014). Still, how these L6 CTs might perform these various functions is not well understood. Many questions remain with regards to the nature of CT feedback as a general feature of sensory circuits and whether these same principles hold across different classes of thalamic nuclei.

Prior work using optogenetics to selectively photoactivate L6 CTs in mouse V1 has suggested that L6 CTs exert an inhibitory modulatory influence over the dLGN (Olsen et al., 2012). The dramatic reduction in visual responses recorded in dLGN from photoactivation of V1 L6 CTs (Denman and Contreras, 2015; Olsen et al., 2012) is thought to be mediated by the thalamic reticular nucleus (TRN), which receives collaterals from L6 CTs and in turn provides GABAergic input to other thalamic nuclei, including dLGN. However, these studies were conducted under anesthesia, which has been shown to affect both spontaneous and visually-evoked firing rates in dLGN (Durand et al., 2016), and they did not control the frequency of photoactivation. On the other hand, there have also been seemingly contradictory observations of increased activity with L6 CT photoactivation in the auditory first-order thalamic nucleus vMGB (Guo et al., 2017) and in the carnivore dLGN with different methods for targeting and stimulating corticothalamic feedback (Hasse and Briggs, 2017). Moreover, optogenetically inactivating L6 CTs has mixed effects in dLGN (Denman and Contreras, 2015), suggesting that their natural function is not to invariably suppress their thalamic targets.

An alternative explanation could be that, depending on their level and manner of activation, L6 CTs are capable of either facilitating or suppressing thalamic activity. For instance, slice experiments in the somatosensory system have shown that transient L6 CT optogenetic stimulation induces prolonged suppression of spiking in first-order thalamus VPm, but with higher-frequency (10 Hz) stimulation, thalamic spike outputs ultimately surpass baseline firing rates (Crandall et al., 2015). This frequency-dependence can be explained by the different short-term plasticity characteristics at different synapses in the full corticothalamic circuit, since the competing monosynaptic excitatory and disynaptic inhibitory (via TRN) routes to first-order thalamus are net-facilitating and net-depressing, respectively (Crandall et al., 2015). Excitatory synaptic inputs to dLGN neurons have also been shown to persistently facilitate with moderate-to-high frequency (5-25Hz) electrical stimulation of the corticogeniculate pathway in slice (Granseth, 2004) and in the anesthetized cat (Lindström and Wróbel, 1990). However, it remains to be seen whether the dynamic synapses of the L6 corticothalamic pathways lead to flexible, bi-directional effects on thalamic activity in the visual system and *in vivo*.

Moreover, previous *in vivo* studies have focused solely on the L6 CT pathway to first-order thalamus and have left unexplored the substantial pathway from L6 of rodent primary sensory cortex to higher-order thalamus. Higher-order thalamic nuclei, such as the pulvinar (also known as the lateral posterior nucleus, or LP, in rodents), receive cortical inputs from layers 5 and 6 (Guillery, 1995; Sherman and Guillery, 1998). In rodents, many of the same L6 CTs in V1 that project to dLGN and TRN (specifically those that reside in lower L6) also terminate in the pulvinar (Bourassa and Deschênes, 1995). These L6 CT inputs to higher-order sensory thalamus have many of the same morphological and physiological features as in first-order thalamus (Li et al., 2003a, 2003b; Reichova and Sherman, 2004) and thus are hypothesized to exert similarly “modulatory” influence over both classes of thalamic nuclei (Sherman, 2016; Sherman and Guillery, 1998). Nonetheless, how L6 CTs contribute to higher-order thalamic activity *in vivo*, and whether the facilitating nature of these synapses (Li et al., 2003b;

Reichova and Sherman, 2004) also enables dynamic functional influence, remain unanswered questions.

Results

Sustained L6 CT photostimulation suppresses activity in dLGN and pulvinar *in vivo*

We first investigated how L6 CTs influence spontaneous and visually-evoked activity in their first-order (e.g., dLGN) and higher-order (e.g., pulvinar) thalamic targets. Are previous effects observed in the dLGN with sustained L6 CT photostimulation in anesthetized animal also observed in *awake* mice and do they also extend to the pulvinar? To address these questions, an AAV encoding Cre-dependent ChR2-eYFP was injected into V1 of Ntsr1-Cre GN220 transgenic mice (Methods). Consistent with prior reports of the specificity of the Ntsr1-Cre transgenic line (Bortone et al., 2014; Gong et al., 2007), expression of the ChR2-eYFP fusion protein was specific to V1 layer 6 (Figure 1B). Corticothalamic axons expressing ChR2-eYFP were readily apparent in both dLGN and pulvinar (Figures 1C and S1A), demonstrating that L6 CTs labeled by the Ntsr1-Cre line project to both visual thalamic nuclei.

Single-unit activity was recorded in the visual thalamus of awake, head-fixed mice using high-density, multi-shank microelectrode arrays (Du et al., 2011; Shobe et al., 2015). Probes were coated with lipophilic dye (DiI) in order to visualize electrode tracks and determine which thalamic nucleus was sampled by each shank (Figure 1C). Because the mouse pulvinar is not uniformly innervated by V1 (Beltramo and Scanziani, 2019; Bennett et al., 2019; Zhou et al., 2017), calretinin expression was used to distinguish between pulvinar subdivisions (Figure S1A). Only units recorded from shanks which passed through eYFP-labeled L6 CT axons from V1 in the lateral, calretinin-negative zone of the pulvinar (Zhou et al., 2017) were included for pulvinar analyses (e.g., second shank in Figure 1C), while units recorded more medially were treated separately (e.g., first shank in Figure 1C, Figures S1B and S1C). While mice viewed either square-wave drifting gratings (“Visual trials”, see Methods) or a gray screen (“Blank trials”), ChR2-expressing cell bodies in V1 were stimulated with one second of sustained blue LED light at each of three different intensities (“low”, "medium", and “high”, Figure 1A; see Methods). This allowed direct comparison of visually-evoked and spontaneous firing rates with and without L6 CT photostimulation at different intensities.

Consistent with what has previously been reported in dLGN in anesthetized mice (Denman and Contreras, 2015; Olsen et al., 2012), L6 CT photostimulation at all light intensities significantly suppressed both visually-evoked (Figures 1D-1F) and spontaneous (Figure S1D-S1F) firing rates (n=102 single-units from 8 shanks in 4 animals; Methods) in dLGN of awake mice ($p<=0.002$ for visual trials with vs. without LED in all light conditions; $p=0.004$, 0.002 and <0.001 for blank trials with vs. without low, med and high LED stimulation, respectively; Wilcoxon signed-rank tests). This effect is exemplified by the first example unit in Figure 1D, whose visually-evoked and spontaneous firing rates were suppressed partially by low light and dramatically by high light. Nevertheless, there was heterogeneity among units; for instance, a small subset was dramatically activated at higher light levels, as demonstrated by the second example unit in Figure 1D. Units like this one tended to be close to each other along the

dorsal-ventral axis of dLGN (Figure 1E), suggesting that the direction of their L6 CT modulation may be related to their spatial (retinotopic) position within the nucleus. The extreme positive light modulation of some of these units obscure the average normalized peristimulus time histogram of the population under each of the three light conditions (Figures 1F and S1F). However, individually, 66.67% of units were significantly suppressed by L6 CT photostimulation (see Methods) while only 15.69% were significantly facilitated (Figures 1F and S1F). In uninjected control animals, no dLGN units were significantly facilitated or suppressed (Figures S1I-S1K), demonstrating the observed effects with LED stimulation were due solely to direct manipulation of L6 CT activity. Thus, with some exceptions, the dominant effect of sustained L6 CT photostimulation on first-order visual thalamus dLGN is suppression.

Figure 1. Sustained L6 CT photostimulation suppresses activity in dLGN and pulvinar *in vivo*

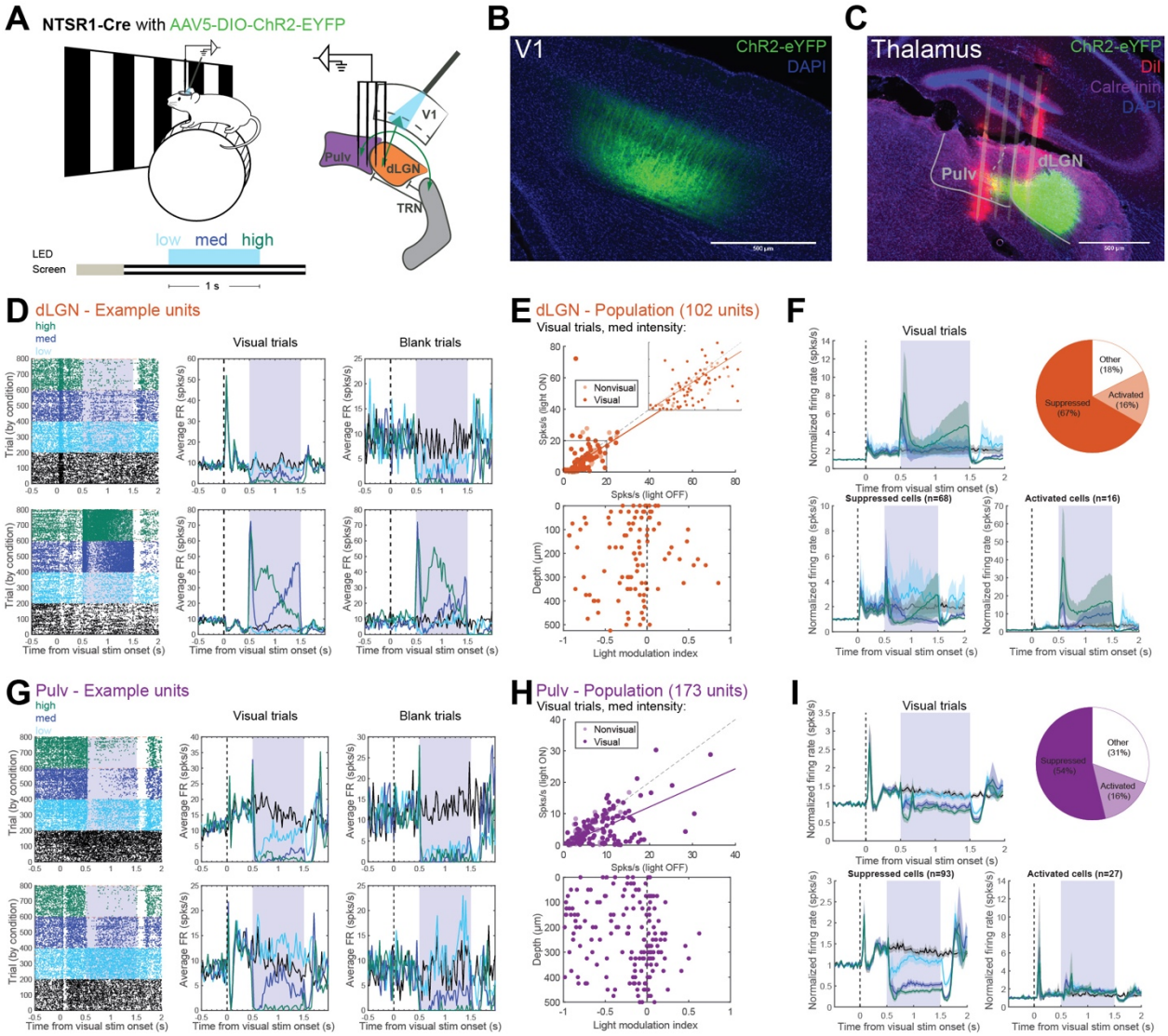

A) Experimental design. Left: diagram of the experimental setup and trial structure for visual and LED stimulation. Right: schematic of the L6 corticothalamic circuit, indicating recording and LED stimulation locations.
B) Coronal section depicting ChR2-eYFP expression in V1 L6 of a Ntsr1-Cre mouse injected with AAV5-DIO-ChR2-eYFP.
C) Coronal section of the visual thalamus, depicting ChR2-eYFP-positive axon terminals in dLGN and pulvinar. Recording tracks from a four-shank probe are labeled with DiI (red). Immunohistochemical staining for calretinin (purple) provides borders between lateral pulvinar and dLGN (calretinin+ axon terminals from retinal ganglion cells) and medial pulvinar (calretinin+ cell bodies).
D) Two example dLGN units. Left panels: raster plots with trials organized by photostimulation condition (trials with different conditions were interspersed during the actual experiment). The shaded area indicates the 1-second photostimulation period (0.5-1.5s following visual stimulus onset). Middle panels: peristimulus time histograms (PSTHs) of average firing rates during visual trials for each photostimulation condition, shown over time relative to visual stimulus onset. Right panels: PSTHs of average firing rates during blank trials (grey screen).
E) Effects of medium-intensity L6 CT photostimulation on visually-evoked firing rates in dLGN. Top: average firing rates during the 1-second photostimulation period from visual trials, with versus without photostimulation. Inset: expanded scatter plot from area within the square (0-20 spks/s). Points are colored according to whether each unit was visually-responsive. Bottom: light modulation index (<0 suppressed, >0 activated) by depth (distance from highest channel on the probe shank with a visually-responsive unit).
F) Effects of different photostimulation intensities on units' visually-evoked activity in dLGN. Top, left: mean normalized PSTH (normalized to each unit's prestimulus firing rate) across all dLGN units. Top, right: proportion of units which were significantly suppressed or activated in two or more photostimulation conditions. "Other" includes units which were not significantly modulated in the same direction (suppressed or activated) in at least two conditions. Bottom, left: average normalized PSTH across suppressed units. Bottom, right: average normalized PSTH across activated units. Shading indicates ± 1 standard error of the mean.
G-I) Same as D-F) but for units recorded in lateral pulvinar.

Since it has been hypothesized that L6 CTs play similarly "modulatory" roles in both first- and higher-order thalamic nuclei (Sherman, 2016; Sherman and Guillery, 1998), it was expected that sustained L6 CT photostimulation would also exert a net-suppressive influence over the pulvinar. Indeed, units recorded in lateral pulvinar (n=173 single-units from 10 shanks in 6 animals) were strongly suppressed by L6 CT photostimulation during visual trials (Figures 1G-1I) as well as blank trials (Figures S1G and S1H) at all light levels ($p<0.001$ for visual trials and blank trials with vs. without LED in all conditions). There was a much higher proportion of visually-responsive units in pulvinar (74.57%) than has been previously reported (Allen et al., 2016), which is likely due in part to our exclusion of units recorded outside of the lateral, V1-recipient zone of pulvinar. (In the calretinin-positive, medial area of pulvinar that lacks direct L6 CT input

from V1, only 42.86% of units were visually-responsive and substantially fewer (30.61%) were modulated by L6 CT photostimulation in either direction (Figures S1B and S1C).) As in dLGN, there was heterogeneity among lateral pulvinar units where some were facilitated, and some even exhibited opposite effects with different light levels (like that depicted in Figure 1G, bottom). The average peristimulus time histogram across units (Figure 1I) illustrates the sustained and graded degree of pulvinar suppression with increasing L6 CT photostimulation intensity. Like in dLGN, significantly suppressed units made up the largest proportion (53.76%) of lateral pulvinar units, while a much smaller proportion (15.61%) was significantly activated (Figure 1I, right). These effects were not observed in pulvinar single-units recorded in uninjected control animals (Figure S1L-M). Thus, we demonstrate for the first time in awake mice *in vivo* that visually-evoked and spontaneous activity in pulvinar, much like in anesthetized and awake (see above) dLGN, is suppressed by sustained L6 CT photostimulation.

L6 CT axon terminal activation in dLGN and pulvinar has different effects from V1 cell body stimulation

Since L6 CT projections are glutamatergic, how do they exert a largely inhibitory influence over their thalamic targets? We noticed that many units exhibited transient facilitation at the onset of L6 CT photostimulation before being subsequently suppressed (e.g., first example unit in Figure 1G; average PSTHs of suppressed cells in dLGN and pulvinar in Figures 1F and 1I), suggesting that feed-forward inhibition is likely involved. Since the rodent dLGN and pulvinar have very few inhibitory interneurons (Evangelio et al., 2018) and those that do exist are rarely innervated directly by corticothalamic inputs (Li et al., 2003a), this fast feed-forward inhibition is likely derived externally.

To test this, we used a two-shank “optrode” (Methods) to record from dLGN and/or pulvinar while directly photostimulating ChR2-expressing L6 CT axon terminals (Figures 2A and 2E). Sustained (1-second) axon terminal stimulation had similar effects on most units recorded in dLGN (Figure 2B) and pulvinar (Figure 2F): a transient increase in firing at stimulation onset, followed by a brief (150-200ms) period of decreased firing, and rebound spiking further followed by either a strong, ramp-like increase in firing rate (Figures 2B and 2F, top examples) or little change (Figures 2B and 2F, bottom examples). In experiments that included at least one shank in dLGN (n=88 single-units from 5 shanks in 4 animals), light levels had to be carefully titrated because runaway activity followed by extended periods of silence were observed if the light intensity was too high (Methods). This likely reflects the much higher density of L6 CT axon terminals in LGN versus pulvinar (Li et al., 2003a). Because of this, lower light levels were used in recordings that included dLGN, and in these instances the ramp-like increase in activity in pulvinar was largely absent (Figures S2A-S2C). Under these stimulation conditions, effects on dLGN activity were variable, with some units having significantly enhanced (27/88) and others suppressed (36/88) activity under the “high” photostimulation condition such that enhancement was not statistically significant at the population level (Figure 2C). Instead, suppression was weak but significant under ramp conditions and in blank trials with low-level light ($p=0.316$, 0.003 and 0.498, visual trials with vs. without low, ramp to high and high LED, respectively; $p=0.002$, <0.001,

Figure 2. Photostimulation of L6 CT axon terminals in dLGN/pulvinar does not suppress activity in visual thalamic nuclei

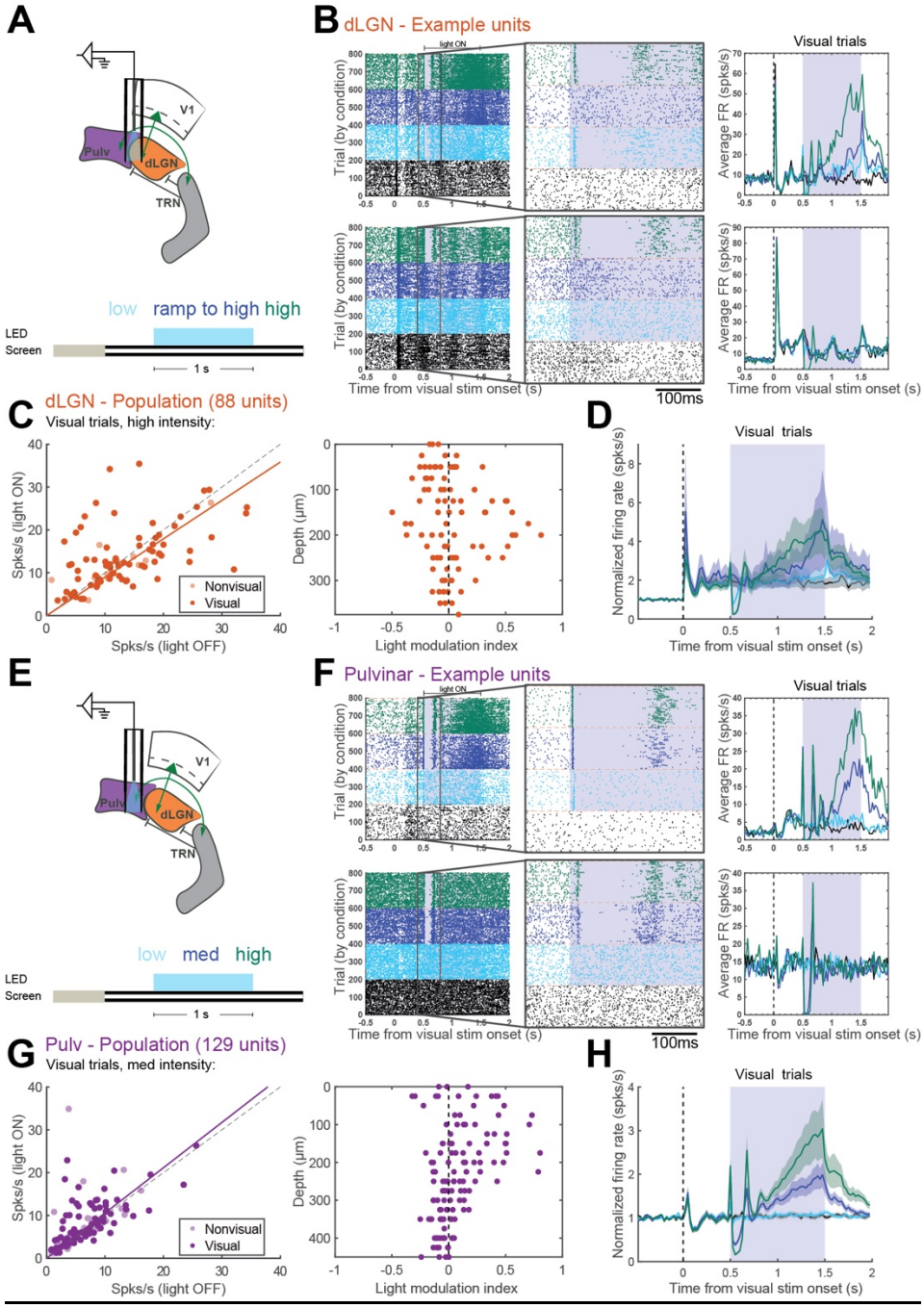

A) Diagram of optrode configuration and trial structure for visual and LED stimulation.
B) Two example dLGN units. Left panels: raster plots. Middle panels: zoomed-in images of boxed parts of raster plots (from 100ms before to 300ms after LED stimulation onset). Right panels: PSTHs of average firing rates during visual trials.
C) Effects of high-intensity L6 CT axon terminal stimulation on visually-evoked firing rates in dLGN. Left: average firing rates during the 1-second photostimulation period

from visual trials, with versus without photostimulation. Right: light modulation index by depth within dLGN.

D) Average normalized PSTH from visual trials across all dLGN units. Shading indicates ± 1 standard error of the mean.

E-H) Same as A-D) but for units recorded in lateral pulvinar, during experiments in which the optrode was entirely in the pulvinar.

0.752, blank trials). In pulvinar-only experiments (n=129 single-units from 6 shanks in 3 animals), higher light levels could be used and resulted in significant enhancement of pulvinar activity (p=0.001, 0.067, <0.001, visual trials with vs. without low, med, and high LED; p=0.185, <0.001, <0.001, blank trials; Figure 2G). In these experiments, 49/129 units were significantly enhanced while only 19/129 were significantly suppressed under the "high" photostimulation condition. As with the subset of facilitated units in cell body stimulation experiments in pulvinar and dLGN, units that were activated by L6 CT axon terminal stimulation in both nuclei were also spatially clustered along the dorsal-ventral axis (Figures 2C and 2G). These effects were not seen in an optrode recording from an uninjected control mouse (Figures S2D-S2F), demonstrating that they were not due to the light itself or to damage from the optrode. Overall, changes to visually-evoked and spontaneous firing rates with L6 CT terminal stimulation were similar between dLGN and pulvinar (Figures 2D and 2H) and qualitatively very different from those with cell body stimulation (Figures 1F and 1I). Thus, a circuit component outside of dLGN and pulvinar must be responsible for the potent net-suppression observed with sustained L6 CT cell body stimulation.

Visual TRN is engaged by sustained L6 CT cell body photostimulation

The most likely source of inhibition from sustained L6 CT photostimulation is through the thalamic reticular nucleus (TRN). TRN receives axon collaterals from L6 CTs in V1 (Bourassa and Deschênes, 1995) and in turn provides GABAergic input to both dLGN and pulvinar. TRN has been shown to be activated by L6 CTs in slice (Crandall et al., 2015; Olsen et al., 2012) and by L6 CTs in auditory cortex *in vivo* (Guo et al., 2017), but how it is engaged by L6 CT photostimulation in V1 of an awake animal has not been tested. Thus, we recorded single-unit activity in the visual sector of the TRN (visTRN) with the same L6 CT stimulation conditions as were used for dLGN and pulvinar recordings (Figure 3A). As one would expect if recordings were well-targeted to visTRN (Figure 3B), more than half (59.38%) of units were significantly visually-responsive, and many (62.50%) exhibited fast-spiking profiles. This is in contrast to 11.05% and 1.30% detected in dLGN and pulvinar, respectively, using the same criteria for fast-spiking (Methods).

Consistent with the hypothesis that disynaptic inhibition through TRN is largely responsible for suppressing dLGN and pulvinar during sustained L6 CT cell body stimulation, many units in visTRN were rapidly and strongly activated under these same conditions (Figure 3C). At the population level (n=32 single-units from 4 penetrations in 3 animals), both visually-evoked and spontaneous firing rates were significantly increased with L6 CT photostimulation at all light levels during visual trials (Figure 3D; p=0.029, 0.023, 0.003 for low, med, and high LED) and approached significance in

blank trials (p=0.014, 0.05, 0.054). Average visTRN population activity was increased by L6 CT stimulation in a graded manner and for the full duration of the photostimulation period, and the majority (53.13%) of units were significantly activated (Figure 3E). Moreover, TRN activation appeared faster than dLGN/pulvinar suppression (Figure 3E vs. Figures 1F and 1I), which is consistent with monosynaptic versus disynaptic origins of these effects. Therefore, given that visTRN is activated during sustained L6 CT photostimulation and provides GABAergic input to dLGN and pulvinar, L6 CTs' suppressive influence over both visual thalamic nuclei is likely to be a consequence of disynaptic inhibition via TRN.

Figure 3. Sustained L6 CT photostimulation activates units in visTRN

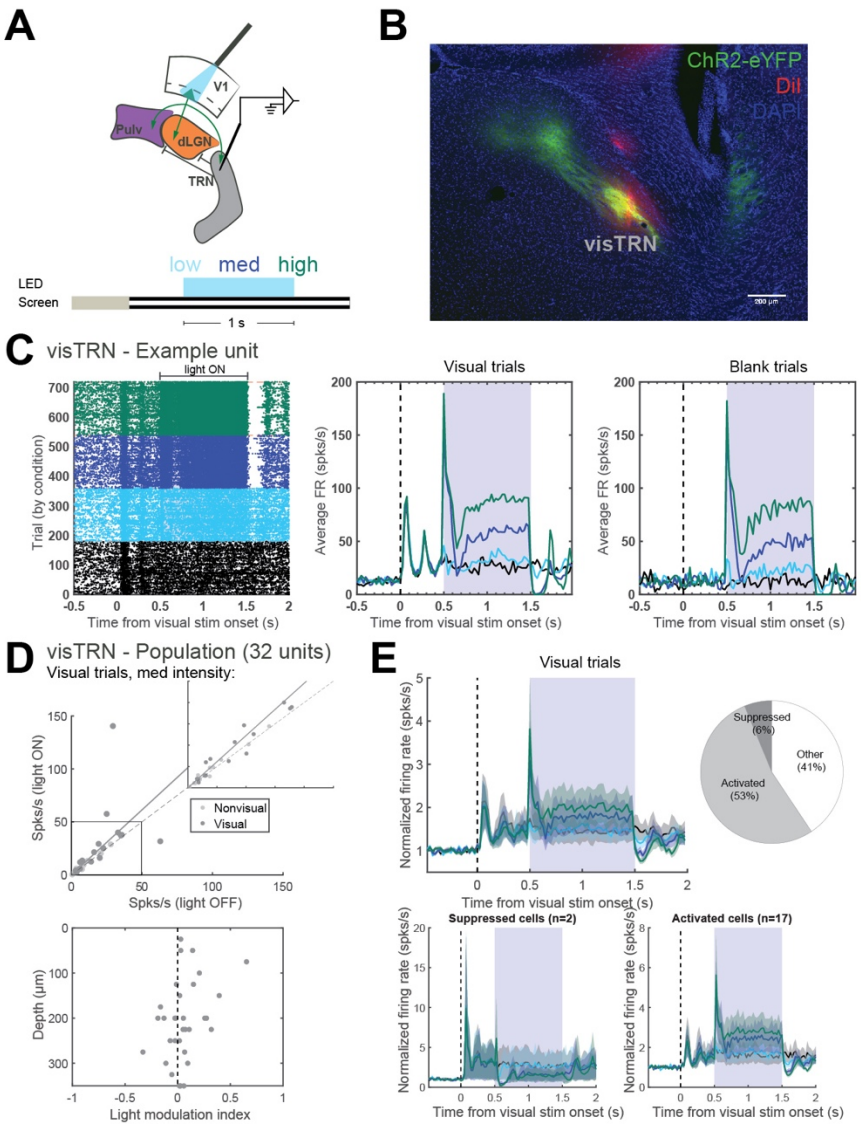

A) Diagram of photostimulation and recording locations and trial structure for visual and LED stimulation.

B) Coronal section depicting ChR2-eYFP-positive axon terminals in the visual sector of the thalamic reticular nucleus (visTRN) from a Ntsr1-Cre mouse injected with AAV-DIO-ChR2-eYFP. The DiI track from the recording probe (red) overlaps with the L6 CT axon terminal field.
C) Raster plot (left) and PSTHs from visual trials (middle) and from blank trials (right) for an example unit recorded in visTRN.
D) Effects of medium-intensity L6 CT photostimulation on visually-evoked firing rates in visTRN. Top: average firing rates during the 1-second photostimulation period from visual trials, with versus without photostimulation. Inset: expanded scatter plot from area within the square (0-50 spks/s). Bottom: light modulation index by depth within visTRN.
E) Effects of different photostimulation intensities on units' visually-evoked activity in visTRN. Top, left: average normalized PSTH across all visTRN units. Top, right: proportion of units which were significantly suppressed or activated in two or more photostimulation conditions. Bottom, left: average normalized PSTH across suppressed units. Bottom, right: average normalized PSTH across activated units. Shading indicates $\pm$1 standard error of the mean.

<u>Frequency-dependent effects of L6 CT photostimulation on dLGN and pulvinar</u>

It has been demonstrated in slice that the different synaptic properties in the direct excitatory and indirect inhibitory pathways from L6 CTs in barrel cortex to first-order thalamus enable them to "switch" from being net-inhibitory to net-facilitatory (Crandall et al., 2015). To test whether these pathways are also frequency-dependent in the visual system and *in vivo*, we used an additional train stimulation paradigm (10ms LED pulses at 1, 10, and 20 or 40 Hz for 1 second) to stimulate L6 CTs during dLGN and pulvinar single-unit recordings (Figure 4A). Recordings with these photostimulation parameters were from the same neurons recorded during sustained photostimulation (above), thus allowing direct comparisons. We hypothesized that, as demonstrated in slice, subsequent stimulation pulses in a 10Hz stimulation train, and perhaps also at higher frequencies, would produce increasing spike outputs due to the facilitating nature of L6 CT synapses and depressing GABAergic input from TRN (Crandall et al., 2015).

Indeed, in both dLGN and pulvinar, we consistently observed facilitating spiking following subsequent pulses in a 10Hz train (Figures 4B and 4G). Whereas a single photostimulation pulse elicited at most a weak response followed by ~150ms of near-complete suppression (1Hz condition), this response increased dramatically with further 10Hz stimulation pulses. Notably, the example pulvinar unit (Figure 4G) is the same unit depicted in Figure 1G (top); while it was strongly suppressed by sustained photostimulation, it exhibited facilitating spiking when driven by 10Hz photostimulation. The facilitation effect across units can be quantified by comparing the number of spikes per unit time following any pulse in the train to the number of spikes after the first pulse; thus, spike count ratios greater than 1 indicate facilitating spiking. Of the units recorded in dLGN and pulvinar that had spiking responses to individual light pulses during 10Hz L6 CT photostimulation (52/102 and 158/173 units considered "Hz-activated" in dLGN and pulvinar, respectively; Methods), the majority had spike count ratios (pulse 2/pulse 1) much greater than 1, and median spike count ratios were greater than 1 for all

subsequent pulses except the last in dLGN (Figures 4C and 4H; asterisks indicate $p<0.005$, sign test). While dLGN and pulvinar spike outputs following L6 CT photostimulation pulses were brief, the duration of these outputs increased from at least the first to the third pulse (Figures 4C and 4H). These signatures of facilitating spiking were absent in laminar recordings from V1 (Figure S3D-S3F), indicating that this phenomenon is specific to L6 corticothalamic (as opposed to intracortical) synapses. Some units (like those depicted in Figures 4B and 4G) also exhibited facilitating spiking at 20Hz, but this was less consistent across units (Figures S4A-S4C). As a population, spike count ratios < 1 (indicating depression) with 20Hz photostimulation were more prevalent, especially in pulvinar; this may be related at least in part to ChR2 kinetics, as 20Hz and faster stimulation of ChR2-expressing somas can lead to reduced probability of successful spikes (Mattis et al., 2011), although such reductions were not observed under our experimental conditions (Figure S4F).

Because of the temporally precise nature of dLGN and pulvinar spike outputs following brief L6 CT photostimulation pulses, the effects of moderate-to-high-frequency photostimulation on average firing rates across the full photostimulation period give an incomplete picture of this pathway's influence. In fact, these average firing rates were, significantly reduced by L6 CT photostimulation in dLGN (Figure 4D: $p=0.014$, <0.001, <0.001 for 1Hz, 10Hz and 20-40Hz in visual trials; p's$<=0.001$ in blank trials) and trending in pulvinar (Figure 4I: $p=0.001$, 0.054, <0.001 in visual trials, $p<0.001$, 0.068 and <0.001 in blank trials). However, the average PSTHs (Figures 4E and 4J) clearly demonstrate the facilitatory effect of 10Hz photostimulation on the populations recorded in dLGN and pulvinar. Moreover, since all dLGN and pulvinar units were recorded under both sustained (Figure 1) and trains (Figure 4) photostimulation paradigms, we were able to directly assess whether facilitating spiking was exclusive to units that were activated by sustained photostimulation or whether suppressed units could also facilitate. Indeed, we found that many units in both nuclei that were significantly suppressed by sustained L6 CT photostimulation exhibited spike facilitation (spike count ratio >1) from 10Hz photostimulation (25/68 and 72/93 in dLGN and pulvinar, respectively) (Figures 4F and 4K). Therefore, moderate-frequency (10Hz) L6 CT photostimulation profoundly facilitates the spiking responses of their thalamic targets – even among those which are suppressed by the same pathway under different conditions.

Moderate-to-high-frequency stimulation of L6 CT axon terminals also had facilitating effects in dLGN and inconsistent effects in pulvinar (Figures S4E-S4J). However, postsynaptic effects of high-frequency stimulation of ChR2-expressing axon terminals is difficult to interpret, as ChR2 has been shown to incompletely recruit axons under moderate-to-high (10-40Hz) stimulation conditions and thus can lead to faulty indications of depressing synapses (Hass and Glickfeld, 2016). Therefore, cell body stimulation experiments are most relevant to the question at hand, and they illustrate strongly facilitating spiking activity in dLGN and pulvinar.

<u>TRN engagement by L6 CT photostimulation is also frequency-dependent</u>

Prior slice experiments have shown that L6 CT synapses onto TRN cells are also facilitating, yet the cumulative effect of the L6 CT-TRN-thalamus pathway is depressing due to TRN's intrinsic burst properties and depressing GABAergic input from TRN onto

thalamic relay cells (Crandall et al., 2015). Consistent with this, we also observed facilitating spike outputs in visTRN recordings in response to 10Hz trains (Figures 4M-4O; $p<0.001$ at $x=1$, $p<0.05$ at $x=3:9$, spike count ratios pulse x/pulse 1), both in terms of the firing rate and duration of spike outputs (Figure 4M). Higher-frequency photostimulation (20Hz) had similar depressing effects on TRN as it did in pulvinar (Figure S4D), which could be due to limitations imposed by ChR2 kinetics (Mattis et al., 2011), TRN's intrinsic burst properties (Crandall et al., 2015), or to other factors that might cause 20Hz to be a non-optimal rate.

Figure 4. 10Hz photostimulation of L6 CTs facilitates spiking in dLGN, pulvinar and visTRN

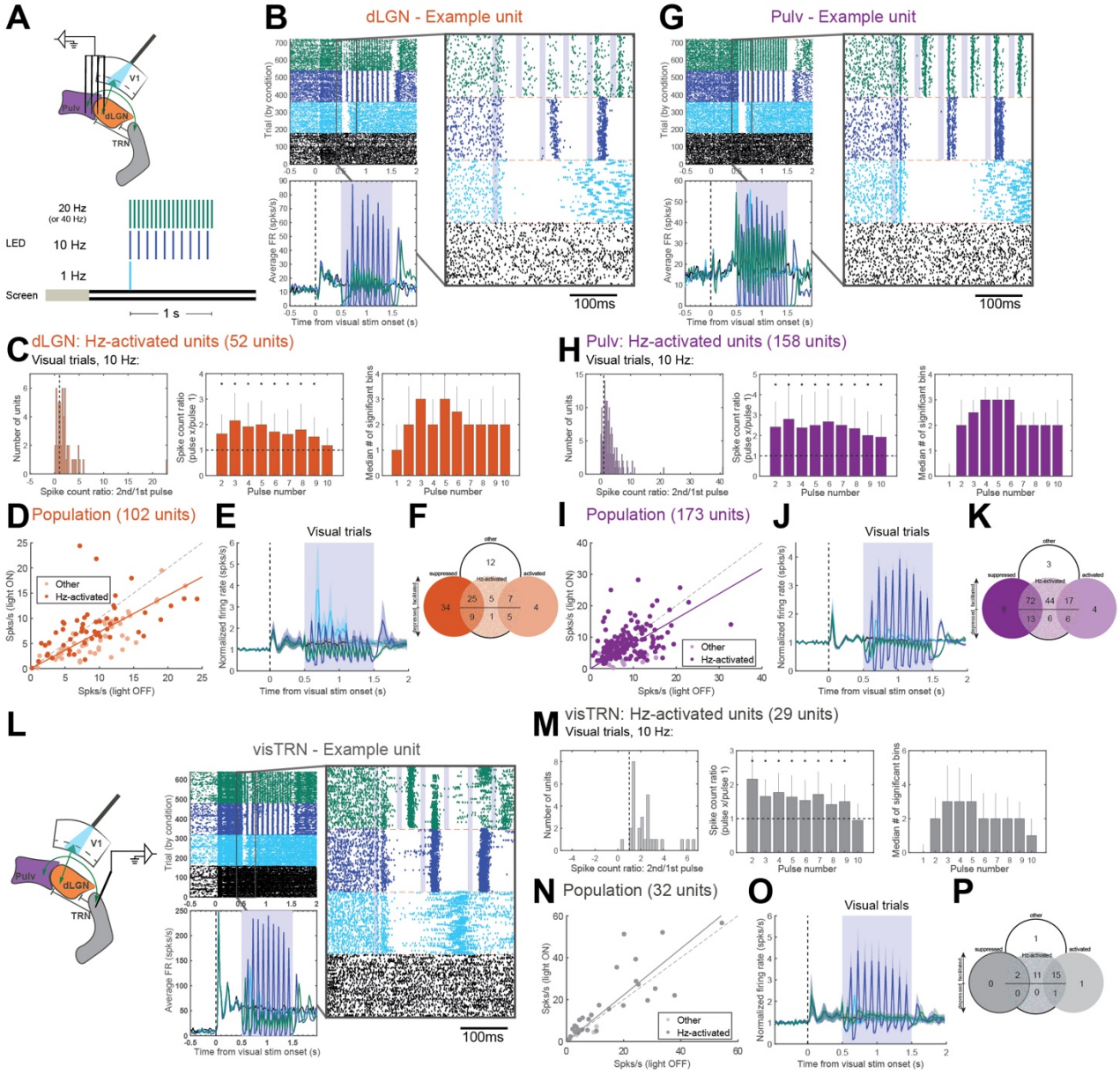

A) Diagram of photostimulation and dLGN/pulvinar recording configuration and trial structure for visual and LED stimulation.
B) An example unit recorded in dLGN. Left: raster plot (top) and PSTH across visual trials (bottom). Right: zoomed-in image of boxed part of raster plot (from 100ms before to 300ms after LED photostimulation onset). Shaded regions indicate photostimulation pulses (10ms duration).
C) Quantification of facilitating spiking during 10Hz photostimulation trials across Hz-activated units in dLGN (see Methods for classification of "Hz-activated" units). Left: histogram of spike count ratios (comparing spike outputs following the second photostimulation pulse relative to the first in a 10Hz train). Middle: median spike count ratios across Hz-activated units, comparing spike outputs following photostimulation pulses 2-10 relative to the first photostimulation pulse. Asterisks indicate ratios significantly different from 1 (p's <0.005, sign test). Right: median number of bins (1 bin = 5ms) in which spike counts were increased after each photostimulation pulse. Error bars indicate interquartile range.
D) Average firing rates during the 1-second photostimulation period from visual trials, with versus without 10Hz photostimulation. Darker points indicate Hz-activated units included in quantification in C).
E) Average normalized PSTH from visual trials across all dLGN units. Shading indicates $\pm$1 standard error of the mean.
F) Venn diagram of "suppressed", "activated", and "other" units (from 1s sustained photostimulation experiments, Figure 1) whose spiking was facilitated (spike count ratio >1), depressed (spike count ratio <1), or not modulated (not "Hz-activated") by 10Hz L6 CT photostimulation.

G-K) Same as B-F) but for pulvinar. Example unit in G) is the same example unit as in Figure 1G (top). Asterisks in H) indicate spike count ratios significantly different from 1 (p's <0.001, sign test).

L-P) Same as B-F) but for visTRN. Asterisks in M) indicate spike count ratios significantly different from 1 (p's < 0.05, sign test).

Overall, the cumulative effect of L6 CT train stimulation on visTRN (Figure 4O) is virtually identical to that on dLGN (Figure 4E) and on the pulvinar (Figure 4J). This is in stark contrast to the results of sustained cell body photostimulation experiments, where the cumulative effect on visTRN (Figure 3E) was opposite of the majority of units in dLGN (Figure 1F) and in the pulvinar (Figure 1I). Thus, depending on the manner of L6 CT photostimulation, dLGN and pulvinar activity is more strongly influenced either by disynaptic inhibition through the TRN or by direct L6 CT inputs. This suggests that these parallel monosynaptic excitatory and disynaptic inhibitory pathways from L6 to first- and higher-order thalamus are dynamically opposed, which leads to highly flexible, context-dependent effects.

Discussion

We set out to investigate how layer 6 corticothalamic neurons (L6 CTs) influence first- and higher-order thalamus, using the visual system as a model. While these corticothalamic neurons are thought to serve modulatory roles in sharpening sensory

responses and enhancing thalamocortical transmission in first-order thalamus (Briggs and Usrey, 2008), how they might accomplish such functions through their different excitatory and inhibitory routes to their thalamic targets is unclear. Moreover, the nature of the pathway from L6 to higher-order thalamic nuclei, like the mouse pulvinar, has not previously been explored, leaving many unanswered questions as to how these corticothalamic neurons might exert similar or dissimilar modulatory control over different classes of thalamic nuclei.

Using high-density multielectrode recordings with optogenetics in awake, head-fixed mice, we find very similar effects on both dLGN and pulvinar with L6 CT photostimulation, but even within nuclei these effects vary drastically depending on the manner and degree of stimulation. Sustained optogenetic activation of L6 CTs in V1 with different levels of light strongly suppresses visually-evoked and spontaneous activity in dLGN and pulvinar, yet controlled 10Hz stimulation of this same population leads to facilitating spiking in both areas. These *in vivo* results in the visual system are strongly reminiscent of the dynamic, frequency-dependent synapses described in the somatosensory thalamocortical slice preparation (Crandall et al., 2015). Remarkably, we also observed similar facilitating spiking at 10Hz in visTRN, yielding virtually indistinguishable effects between TRN and pulvinar/dLGN; this stands in stark contrast to the effects on TRN and pulvinar/dLGN under sustained stimulation conditions, which were opposite in sign. These findings demonstrate the highly dynamic nature of these connections, whereby the relative balance between monosynaptic excitatory and disynaptic inhibitory (via TRN) pathways from L6 of V1 to pulvinar and dLGN can shift depending on the context of corticothalamic engagement. These patterns of activity are also likely to be strongly influenced by the reciprocal excitatory/inhibitory connections between the TRN and both dLGN and pulvinar (Conley and Diamond, 1990; Jones 1985). Therefore, describing the overall effect of the L6 corticothalamic pathway on dLGN and pulvinar as simply suppressive or excitatory would fail to capture the functional nuance of this circuit.

Previous optogenetic experiments using Ntsr1-Cre transgenic mice under anesthesia describe a net-suppressive influence of sustained L6 CT activation on first-order visual thalamus dLGN (Denman and Contreras, 2015; Olsen et al., 2012). We replicate these findings in awake mice and show similar effects in the pulvinar. However, we also observed a handful of spatially-clustered units, especially in dLGN, that were dramatically activated by higher-level photostimulation, yet many of these same units were suppressed by low-level L6 CT stimulation (e.g., second example unit in Figure 1D). Conversely, some units, like the second example pulvinar unit in Figure 1G, were suppressed at higher light levels but activated by low light (also evident in the population of suppressed dLGN units, Figure 1F). While we still find significant population-level suppression of thalamic activity with each of our chosen light intensities, the heterogeneity of single-unit responses to different degrees of sustained L6 CT photostimulation, together with the frequency-dependent effects we observed using photostimulation trains, highlight the complex nature of L6 corticothalamic circuitry that is not simply unidirectional. It should be noted as well that our use of full-field visual stimuli, broad activation of L6 CTs throughout V1 and simultaneous single-unit recordings from different retinotopic locations in thalamus may bias us toward seeing suppressive effects, as some evidence suggests that inhibition is broader than

retinotopically-aligned excitation in dLGN (Tsumoto et al., 1978). Nevertheless, we find that the effects of L6 CTs on their first- and higher-order thalamic targets are not merely inhibitory but instead depend critically on the context of their activation.

A particularly novel aspect of our work is our assessment of the functional influence of L6 CTs on the rodent pulvinar. We find that L6 CTs provide considerable inhibition (putatively through TRN) to the pulvinar, as they do to dLGN, and that their routes from L6 to both nuclei are highly dynamic. The similarities in these corticothalamic pathways to first- and higher-order visual thalamus are consistent with prior observations of similar morphological (Bourassa and Deschênes, 1995; Li et al., 2003a) and physiological (Li et al., 2003b; Reichova and Sherman, 2004) characteristics of L6 CT inputs to both classes of sensory thalamic nuclei. From this type of evidence, it has been hypothesized that L6 CT inputs from visual cortex provide similarly "modulatory" input to the pulvinar as they do to dLGN, whereas pulvinar's "driving" input comes from layer 5 (L5) CT neurons that project exclusively to higher-order nuclei (Sherman, 2016; Sherman and Guillery, 1998). Our findings are thus in line with this hypothesis, although the relative contribution of L5 inputs to pulvinar compared to the L6 CT pathways described here remains to be tested.

In some ways, it is surprising that the L6 CT manipulations used in this study had as profound an effect on the pulvinar as they did. Though many L6 CTs that project to dLGN also project to the pulvinar (Bourassa and Deschênes, 1995), those that project to both classes of thalamic nuclei are only found in lower L6 (Bourassa and Deschênes, 1995; Bourassa et al., 1995; Chevée et al., 2018; Roth et al., 2016). The pulvinar receives L6 inputs from other visual cortical areas as well, and pulvinar-projecting L6 CTs in these areas are found throughout L6 (Roth et al., 2016). Thus, by restricting photostimulation to V1, we may be engaging a subset and perhaps even a minority of the pulvinar's L6 CT inputs, yet we see robust effects of L6 CT photostimulation that are very similar to what we see in dLGN. Moreover, a recent study identified a small population of L6B cells that project exclusively to higher-order thalamus, but not to first-order thalamus or TRN (Hoerder-Suabedissen et al., 2018); if and how this population's functional influence on pulvinar differs from that of the more common L6 CT population would be of significant interest. We cannot rule out the possibility that the suppressive influence of L6 CTs on other cortical populations within V1 (Olsen et al., 2012), including the putative "driving" inputs from L5 to pulvinar, also contributes to the inhibitory effects we see in pulvinar with sustained L6 CT photostimulation. However, we note that L5, including lower L5 ("L5B") where subcortically-projecting L5 neurons in V1 are somewhat biased to reside (Groh et al., 2010), was not fully inactivated under our light stimulation conditions (Figure S3C).

Our results contribute to a broader understanding of the circuit computations underlying L6 CTs' putatively "modulatory" functions in both first- and higher-order sensory thalamus. Observations of visual response suppression by L6 CTs in dLGN (Denman and Contreras, 2015; Olsen et al., 2012) has led some to suppose that this is the primary mechanism by which these corticothalamic neurons wield functional influence over their thalamic targets. However, our results suggest that L6 CTs take a more nuanced approach. We propose that L6 CTs can exert net-inhibition over their thalamic targets under some conditions – such as when only transiently or weakly activated, or when activated non-optimally (e.g., 20Hz or higher for many recorded

units) – and in others can facilitate their targets' responses to their inputs. The precise conditions that lead to inhibition versus facilitation are likely to vary between dLGN and pulvinar due to the higher density of L6 terminals in dLGN than in pulvinar (Li et al., 2003a); this is supported by our observations that a) L6 CT cell body photostimulation more strongly activated a subset of units in dLGN than in pulvinar (Figures 1F and 1I), and b) L6 CT axon terminal stimulation caused a ramp-like increase in many dLGN units (Figure 2) while having little net effect on simultaneously-recorded units in pulvinar (Figure S2).

The balancing act between excitatory and inhibitory CT pathways that we describe could support stimulus-specific amplification in the thalamus (Briggs and Usrey, 2008; Granseth, 2004). For instance, a given L6 CT neuron that is optimally activated (~10Hz) by its preferred visual stimulus in its receptive field provides facilitating excitatory drive to its thalamic relay cell targets, whereas weaker activation (e.g., by a less-preferred and/or retinotopically misaligned stimulus) may result in net-suppression. In fact, L6 CTs in mouse have been shown to have low spontaneous firing rates but to be highly orientation-tuned (Vélez-Fort et al., 2014), which suggests that their firing rates vary considerably in response to different stimuli under normal physiological conditions. Moreover, prior studies in cat dLGN suggest precise alignment of corticothalamic feedback excitation with potentially wider inhibition (Tsumoto et al., 1978; Wang et al., 2006). While our use of broad L6 CT activation throughout V1 and simultaneous single-unit recordings across different retinotopic locations in dLGN and pulvinar prohibits us from directly assessing whether stimulus-specific amplification through frequency-dependent synapses was at work, this idea is supported by the observation of sharpened spatiotemporal receptive fields in dLGN with retinotopically-aligned L6 CT photostimulation (Hasse and Briggs, 2017). This hypothesis may further extend to higher-level representations, particularly with regards to the pulvinar. For instance, computational modeling demonstrates that frequency-dependent synapses in parallel excitatory and inhibitory pathways from cortex to pulvinar can enable representations of perceptual decision confidence in the pulvinar (Jaramillo et al., 2019). With an improved understanding of the highly dynamic nature of these L6 corticothalamic pathways to first- and higher-order thalamus in an awake animal, future work may be able to elucidate their role in modulating sensory processing in the context of sensory-guided behaviors.

Acknowledgements: We thank Ashley Juavinett for comments on the manuscript, Sotiris Masmanidis and Kwang Lee for help with optrode assembly, and other members of the Callaway lab for helpful discussions. This work was supported by NIH grants F31 EY028853 (M.A.K.) and R01 EY022577 (E.M.C.).

Contributions: Conceptualization, M.A.K. and E.M.C.; Methodology, M.A.K. (optogenetics and electrophysiology) and A.D.F. (histology); Investigation and Formal Analysis, M.A.K.; Data Curation (spike-sorting), M.A.K. and A.D.F.; Writing – Original Draft, M.A.K.; Writing – Review and Editing, M.A.K., A.D.F. and E.M.C.; Funding Acquisition, M.A.K. and E.M.C.; Resources and Supervision, E.M.C.

Declaration of Interests: The authors declare no competing interests.

Methods

Contact for reagent and resource sharing

Further information and requests for resources and reagents should be directed to and will be fulfilled by the Lead Contact, Edward Callaway (callaway@salk.edu).

Experimental model and subject details

Male and female Ntsr1-Cre GN220 transgenic mice (GENSAT) aged 8-14 weeks (with the exception of three mice, which were 16-17 weeks old) were used for experiments. Cre-negative animals were used for control experiments. All experimental procedures followed protocols approved by the Salk Institute Animal Care and Use Committee.

Method details

Surgeries

Mice were first anesthetized with a ketamine/xylazine cocktail (100mg/kg of ketamine and 10 mg/kg xylazine) via intra-peritoneal injection and then placed in a stereotax (David Kopf Instruments Model 940 series). A small craniotomy was made over primary visual cortex of the left hemisphere (coordinates relative to bregma: 3.20mm posterior, 2.65mm lateral). A total of 100-150nl of AAV5-EF1a-DIO-hChR2(H134R)-eYFP was pressure-injected via Picospritzer (General Valve Corp) or syringe through a 25-30μm pipette at 1-2 depths, 0.3-0.6mm from pial surface. Viruses were injected at an approximate rate of 20nl/min, and the pipette was left in place for at least 5 minutes following injection prior to removal. Mice were returned to their cages and given 2.5-3 weeks before experimentation.

Four to seven days before experimentation, mice underwent an acute surgery for headframe implantation. Skin was cleared away so that a circular headframe (7mm inner diameter) could be attached with dental cement (C&B-Metabond, Parkell). A dull pipette attached to a micromanipulator (MP-285, Sutter Instrument Co) was used to relocate bregma and mark positions with a waterproof pen for targeting thalamus recordings (coordinates relative to bregma: 1.25-2.75mm lateral, 1.8-1.9mm posterior). The skull was covered with a silicone elastomer (Kwik-Cast, World Precision Instruments) and mice were given a carpofen subcutaneous injection (5mg/kg), Ibuprofen in their water bottles and at least 24 hours undisturbed in their cages.

In vivo electrophysiology

Prior to recordings, mice were given 2-4 training sessions to habituate to the running wheel. One day prior and on the day of recordings, mice were given a dilution of dexmethasone (15mg/kg) to alleviate brain swelling. On the day of recording, mice were anesthetized with isoflurane and a craniotomy was made over the thalamus of the left hemisphere. For cell body stimulation experiments, an additional craniotomy was made over the injection site in V1 (in two animals the cortex was heavily thinned). Mice were then head-fixed on a wheel, where they were free to run at their will and movement was tracked with a rotary encoder. Silicon microprobes (Du et al., 2011; Shobe et al., 2015) were coated with a 2.5-5% solution of DiI (D282, ThermoFisher) in distilled water or ethanol and lowered into thalamus with a micromanipulator (MP-285, Sutter Instrument

Co). Probe configurations were: 128DN (128 channels across 4 shanks, 150µm separation between shanks, 775µm vertical extent of electrode contacts), 128D (same as 128DN but 330µm separation between shanks), and 64G (64 channels across 2 shanks, 300µm separation between shanks, 525µm vertical extent of electrode contacts). For cell body stimulation experiments, a 1mm diameter optical fiber (1mm diameter, 0.39 NA, ThorLabs) was positioned at approximately a 50-60° angle from and 0.5-1mm above the surface of the V1 craniotomy. Multi-shank probes for thalamic recordings were oriented horizontally (medial-lateral). After the probe penetrated the cortical surface, agarose (2.5-3.5%; A9793, Sigma-Aldrich) was poured over to fill the well of the headframe holder, thus covering the probe shank(s) and the tip of the optical fiber. The probe was continuously lowered slowly down to ~2.4-2.6mm beneath the cortical surface over the course of approximately 20 minutes. Once the probe was in its final position, it was allowed to sit and settle for 30 minutes before any data acquisition commenced. Data from all but two animals was acquired at 20kHz with an OpenEphys acquisition system (Siegle et al., 2017), connected to an Intan RHD2000 128-channel amplifier board. Data from the remaining two animals was acquired at 20kHz with an Intan RHD2000 USB interface board.

Visual and optogenetic stimulation

Visual stimuli was generated through custom MATLAB code using Psychtoolbox, as described previously (Marshel et al., 2011) and presented on a 24" LED monitor (GL2450-B, BenQ). The monitor screen was positioned 12cm from the mouse's right eye. Visual stimuli consisted of square-wave drifting gratings at four orientations in eight directions, 0.04 cycles/° spatial frequency, 2Hz temporal frequency (one experiment in one mouse at 1Hz). A full "trial" consisted of a 0.5-second pre-stimulus period (grey screen), 2 seconds of visual stimulus presentation, and 1.5-2 seconds post-stimulus period (grey screen). 20% of trials were "blank" trials, in which the screen remained grey for the full trial duration.

Optogenetic stimulation was controlled via an Arduino Zero microcontroller board with a 12-bit DAC output pin. The Arduino interfaced with the visual stimulus generator code through a serial port connection to read in input parameters for start time, duration, intensity and frequency of LED stimulation from a custom Matlab GUI. All experiments consisted of a "no light" condition plus three different light conditions: sustained photostimulation at low, medium, or high light intensities, or trains of 10ms photostimulation pulses at 1, 10, and 20 Hz (40 Hz in two mice). All recorded units underwent both sustained and trains photostimulation experiments. LED stimulation always lasted for 1 second and started 1 second after the trial start (0.5 seconds after visual stimulus onset). For cell body stimulation experiments, blue LED light was delivered through a custom optical fiber patch cord (1mm diameter, 0.39 NA, ThorLabs) connected to an LED driver (PlexBright LED 465nm, Plexon) positioned at approximately a 50-60° angle from and 0.5-1mm above the surface of the V1 craniotomy. For axon terminal stimulation experiments, blue light was delivered through a custom "optrode" (64G probe, integrated with a 200µm diameter, 0.22 NA multimode fiber halfway between the two shanks and ending just above the top contacts) connected to an LED driver (470nm fiber-coupled LED with T-Cube LED driver, ThorLabs). Light intensity was controlled by assigning output values for the Arduino

DAC 12-bit output pin (0-4095). These output values were typically kept consistent across experiments, but power output was also measured with a power meter (PM100D with S121C power sensor, ThorLabs) as verification of consistency. Output power ranges from the Plexon LED through the 1mm diameter fiber were 0.7-1mW ("low"), 3.5-4.5mW ("med"), and 6.5-8.5mW ("high"). Output powers from ThorLabs LED to optrode with 200µm diameter fiber were estimated with a dummy fiber-optic implant (200µm diameter, 0.22NA). In these optrode experiments, DAC outputs assigned to "low", "med" and "high" conditions had to be varied by experiment because it was observed in some experiments, and specifically in experiments in which at least one shank on the probe was in dLGN, too high light power caused a massive ramp-like increase in activity before units went completely silent for >20 seconds. Thus, light levels were titrated during recording so that this seemingly excitotoxic effect did not occur. Consequently, estimated light levels during experiments that included at least one shank in dLGN ranged from 120-152µW ("low") and 250-560µW ("high") as measured through the 200µm diameter dummy fiber. In these experiments, the third light condition was a 1 second ramp, in which the Arduino DAC output was linearly increased in bits over 1 second so that it ended at the "high" light level. In pulvinar-only optrode experiments, estimated light levels ranged from 120-152µW ("low"), 250-310µW ("med") and 500-600µW ("high").

Histology

After recordings were completed, animals were given an intraperitoneal injection of euthasol dilution (15.6mg/ml) and then perfused with phosphate-buffered saline (PBS) followed by 4% paraformaldehyde. Brains were dissected out from skulls and post-fixed in 2% PFA and 15% sucrose solution at 4°C for ~24 hours before being moved to 30% sucrose at 4°C for at least another ~24 hours. Brains were frozen in sucrose and sliced on a freezing microtome into 50µm sections, starting from anterior edge of the hippocampus to the posterior end of cortex. All sections were counterstained with 10µM DAPI in PBS for 10 minutes before being mounted and coverslipped with Polyvinyl alcohol mounting medium containing DABCO. Additional immunohistochemistry was performed on thalamic sections by incubating at 4°C for 16-20 hours with rabbit anti-calretinin primary antibody (1:1000; Swant 7697) in 1% Donkey Serum/.1% Triton-X 100/PBS, followed by donkey anti-rabbit conjugated to Alexa 647 (1:500; A-31573, Life Technologies) before DAPI counterstaining. Imaging was performed with an Olympus BX63 microscope with a 10X objective.

Spike sorting

Spike-sorting on extracellularly recorded data was performed semi-automatically using Kilosort (Pachitariu et al., 2016). Briefly, different recordings from the same recording session (e.g., different intensities experiment followed by trains stimulation experiment) were concatenated together into a single binary file, common average referenced, bandpass filtered (300-2000Hz) and spatially whitened prior to template-matching. Because onset and offset of LED stimulation for optogenetics caused artifacts that could be mistaken for spikes by the algorithm, spikes within 3ms of the light onset and offset were removed, and additional "spikes" were removed whose amplitudes surpassed 20 times the standard deviation of spike amplitudes. Clusters were further

curated manually using Phy (Rossant et al., 2016). Additional optogenetic artifacts were usually evident as points far outside the cluster of principal component features whose cross-correlograms with their assigned clusters exhibited clear refractory period violations and thus could be manually removed. For a few experiments in which the timing of the ADC input to OpenEphys from the Arduino (for controlling the LED) was not saved properly due to a bug in the OpenEphys GUI, thus prohibiting us from removing optogenetic artifacts based on their timing relative to LED onset and offset, we removed artifacts based only on their large amplitudes in Kilosort and as outliers in their principal component features in Phy. If artifacts were not removed, they were extremely obvious in unit raster plots because they lined up precisely with LED photostimulation onset/offset and thus were readily distinguishable from legitimate spikes, even those with short latency. Thus, we are very confident that we successfully removed the vast majority of optogenetic artifacts, and all short-latency responses that we report come from legitimate spikes. We did our best to also remove optogenetic "hash" from ChR2-expressing axons, which usually manifested as points well outside the main cluster in the principal component features view that exhibited substantial refractory period violations in their cross-correlograms. These "hash"-y units were especially prominent in dLGN and, when analyzed separately, their spikes occurred nearly exclusively during photostimulation periods, further suggesting that they were not true thalamic units (which had high spontaneous firing rates). Spike clusters were manually assigned to noise, multi-unit, and good/single-unit categories, and only good single-units that had fewer than 0.5% refractory period violations and "unit quality" (isolation distance; method from (Schmitzer-Torbert et al., 2005), MATLAB code adapted from https://github.com/cortex-lab/sortingQuality) greater than 16 were included for analyses.

Assigning units to thalamic nuclei

Prior to *in vivo* recordings, recording probes were coated in DiI and were easily visualized post-mortem. Staining for calretinin (described above) provided a clear border between lateral pulvinar (calretinin-negative) and dLGN (calretinin-positive axons from retinal ganglion cells), thus allowing for definitive assignment of units recorded on different probe shanks to lateral pulvinar or dLGN. In rare instances, a DiI trace fell ambiguously right on the border between pulvinar and dLGN, in which case units recorded from the corresponding shank were excluded from analyses. Calretinin staining also provided an additional border between lateral pulvinar and rostral-medial and caudal-medial pulvinar, were cell bodies were calretinin-positive. Pulvinar units were assigned to lateral pulvinar if the DiI trace from their corresponding probe shank passed through the calretinin-negative portion of pulvinar and through eYFP-positive axon terminals, whereas shanks passing mainly through calretinin-positive cells and absent or sparse eYFP-expressing axons were considered in medial pulvinar. Calretinin staining did not allow us to distinguish between rostromedial and caudomedial pulvinar (Zhou et al., 2017).

To approximate where the dorsal/ventral boundaries of thalamic nuclei (dLGN, pulvinar, visTRN) fell on each recording shank, we determined the anatomical boundaries of visually responsive units. To identify visually responsive units, we identified the visual direction which maximally changed each unit's firing rate from

baseline and used the spike counts from those preferred visual stimulus trials without LED stimulation to assess whether each unit's activity was significantly different from "blank" trials without LED stimulation (Wilcoxon rank-sum test). We separately compared spike counts between blank and preferred-visual trials during the first 100ms of the visual stimulus (to assess visual onset response) and 0.5-1.5s from the visual stimulus onset (to assess sustained visual stimulus response), and thus considered units visually-responsive if either of these p-values passed the 0.025 threshold (Bonferroni correction for two comparisons). We then estimated the dorsal/ventral boundaries of visual thalamic nuclei as the first and last channels on each probe shank which had visually responsive units. These boundaries were corroborated across experiments from the same recording sessions, and if there were discrepancies the boundaries were set as those channels which had significantly visually responsive units in both experiments. In this way, all units analyzed from sustained photostimulation experiments were also analyzed for the trains experiments and vice versa. For visTRN recordings, we sometimes recorded visually-responsive units very far ventral and with very short latency, possibly through the optic tract. Thus, we also included as criteria that channels with visually-responsive units that were separated by more than 100μm from the nearest visually-responsive channel were excluded, and for visTRN specifically that depth of included channels should not exceed 400μm. Units were considered fast-spiking (FS) whose waveform trough-to-peak times were less than 0.4ms but were not analyzed separately because they were very uncommon in dLGN and extremely rare in pulvinar, consistent with other reports (Durand et al., 2016).

V1 recordings

In two mice, additional experiments were performed to record single-unit activity in primary visual cortex with a single (64D) recording probe, while a few mice (n=3) only underwent V1 recordings with a two-shank (128AN) recording probe. The same optogenetic and visual stimulation conditions were used as for thalamic recordings, but with an additional stimulus protocol consisting of alternating 2-second periods of screen-on and screen-off for 2 minutes. From these short recordings, we performed current source density (CSD) analysis by taking the second spatial derivative using CSDPlotter (Pettersen et al., 2006) of the low-pass-filtered (<1000Hz) local field potential during the transitions between screen-off and screen-on periods. For each column of each shank, we assigned channels to layer based on the following criteria: congruent channels which exhibited the fastest current sink (typically 2-3 channels per column, spanning 100-150μm) were assigned to layer 4; those that fell above this initial current sink as layer 2/3; those that exhibited an additional but delayed current sink starting approximately 150-300μm beneath the bottom of layer 4 as layer 5B; those in between layers 4 and 5B and layer 5A; and those below layer 5B as layer 6. Units were separated into fast-spiking (FS) and regular-spiking (RS) categories based on their waveform trough-to-peak times (<0.475ms considered FS) because this metric appeared to clearly separate all recorded units into two main clusters. Firing rates and light modulation indices were analyzed as for thalamic units.

Quantification and statistical analysis

Analysis of optogenetic effects on firing rates

Average firing rates were calculated from the one-second period of photostimulation (0.5-1.5s from visual stimulus onset). Mice were on a treadmill but did not run very often. Regardless, we exclusively used stationary trials (speed < 2cm/s) for our average firing rate calculations since running has been shown not only to affect firing rates in V1 (Niell and Stryker, 2010), but also in dLGN (Erisken et al., 2014). Firing rates were calculated separately for visual and blank trials and for each light condition (no light, low, med, high).

For population-level statistics on the effects of L6 CT photostimulation on these average firing rates, we pooled together all units from the same experiment type (e.g., trains vs. sustained photostimulation) and from the same thalamic nucleus (e.g., pulvinar) across animals and recording shanks and compared their firing rates in trials without L6 CT photostimulation to firing rates in each photostimulation condition using the Wilcoxon signed-rank test. Population-averaged peristimulus time histograms (PSTHs) were constructed using individual units' average firing rate across trials (visual and blank trials separately) in 25ms bins across the full trial duration (2.5s). We then normalized to each unit's baseline firing rate (calculated from the 500ms prestimulus period) and averaged these normalized PSTHs across units.

Average firing rates were also used to compute a light modulation index for each unit. The light modulation index was computed as the difference between average firing rates in visual trials with and without L6 CT photostimulation (separately for each photostimulation condition) divided by their sum. Thus, a light modulation index greater than 0 indicates increased activity with L6 CT photostimulation while less than 0 decreased activity.

To determine the statistical significance of each unit's response to L6 CT photostimulation, we compared spiking responses during the one second photostimulation period on all trials with and without photostimulation (separately for each photostimulation condition) with a Wilcoxon rank-sum test. In order to summarize how individual units were affected by sustained L6 CT photostimulation across all photostimulation conditions (low, medium, and high intensities), units were considered "suppressed" if their activity was significantly suppressed ($p<0.05$ and light modulation index < 0) in at least 2/3 conditions, or "activated" if their activity was significantly increased ($p<0.05$ and light modulation index >0) in at least 2/3 conditions.

Analysis of frequency-dependent effects

First, since it was not expected that every neuron we recorded from should be directly innervated by our ChR2-expressing L6 CTs (as demonstrated by non-uniform expression of ChR2-eYFP across each thalamic nucleus), we first sought to identify units that spiked in response to individual photostimulation pulses. With each unit's peristimulus time histogram of spike counts (in 5ms bins) for visual trials with 10Hz or 20Hz photostimulation, we used the following criteria for so-called "Hz-activated" units: 1) at least one bin surpasses threshold (three standard deviations above the mean visually-evoked response, taken from the one-second photostimulation period in no light trials) within 50ms of at least the first or second photostimulation pulse in the train; 2) if there was no significant response to either of the first two photostimulation pulses, there had to be significant response bins (above threshold) following at least half of all

subsequent pulses. Only these “Hz-activated” units were analyzed for paired-pulse ratios and spike output durations.

Spike count ratios were calculated as the mean number of spikes per bin (averaged across significant bins within 50ms of photostimulation) following each photostimulation pulse, divided by the mean spike response to the first pulse. In the absence of any response bins crossing threshold after the first photostimulation pulse, we took the maximum bin within 50ms of photostimulation onset. This was a conservative approach so that, if anything, we would underestimate paired pulse ratios (since we would likely be overestimating the spiking response to the first pulse). In the absence of significant bins after any of the following photostimulation pulses, we took the mean spike response across all bins within 50ms of pulse onset. The number of 5ms bins that crossed threshold for significant spike responses was also calculated as a measure of spike output duration. Since the distributions of these data were clearly non-normally distributed, we chose to plot the medians and interquartile ranges. The sign test was used to test the null hypothesis that the median of spike count ratios was equal to one (i.e., no change in spike outputs).

Data and software availability

Data and analysis code will be made available upon reasonable request.

References

Allen, A.E., Procyk, C.A., Howarth, M., Walmsley, L., and Brown, T.M. (2016). Visual input to the mouse lateral posterior and posterior thalamic nuclei: photoreceptive origins and retinotopic order. J. Physiol. (Lond.) *594*, 1911–1929.

Andolina, I.M., Jones, H.E., Wang, W., and Sillito, A.M. (2007). Corticothalamic feedback enhances stimulus response precision in the visual system. Proc. Natl. Acad. Sci. USA *104*, 1685–1690.

Andolina, I.M., Jones, H.E., and Sillito, A.M. (2013). Effects of cortical feedback on the spatial properties of relay cells in the lateral geniculate nucleus. J. Neurophysiol. *109*, 889–899.

Beltramo, R., and Scanziani, M. (2019). A collicular visual cortex: Neocortical space for an ancient midbrain visual structure. Science *363*, 64–69.

Bennett, C., Gale, S.D., Garrett, M.E., Newton, M.L., Callaway, E.M., Murphy, G.J., and Olsen, S.R. (2019). Higher-Order Thalamic Circuits Channel Parallel Streams of Visual Information in Mice. Neuron *102*, 477–492.e5.

Bortone, D.S., Olsen, S.R., and Scanziani, M. (2014). Translaminar inhibitory cells recruited by layer 6 corticothalamic neurons suppress visual cortex. Neuron *82*, 474–485.

Bourassa, J., and Deschênes, M. (1995). Corticothalamic projections from the primary visual cortex in rats: a single fiber study using biocytin as an anterograde tracer. Neuroscience *66*, 253–263.

Bourassa, J., Pinault, D., and Deschênes, M. (1995). Corticothalamic projections from the cortical barrel field to the somatosensory thalamus in rats: a single-fibre study using biocytin as an anterograde tracer. Eur. J. Neurosci. *7*, 19–30.

Briggs, F., and Usrey, W.M. (2008). Emerging views of corticothalamic function. Curr. Opin. Neurobiol. *18*, 403–407.

Chevée, M., Robertson, J.D.J., Cannon, G.H., Brown, S.P., and Goff, L.A. (2018). Variation in activity state, axonal projection, and position define the transcriptional identity of individual neocortical projection neurons. Cell Rep. *22*, 441–455.

Conley, M., and Diamond, I.T. (1990). Organization of the visual sector of the thalamic reticular nucleus in galago. Eur. J. Neurosci. *2*, 211–226.

Crandall, S.R., Cruikshank, S.J., and Connors, B.W. (2015). A corticothalamic switch: controlling the thalamus with dynamic synapses. Neuron *86*, 768–782.

Denman, D.J., and Contreras, D. (2015). Complex Effects on In Vivo Visual Responses by Specific Projections from Mouse Cortical Layer 6 to Dorsal Lateral Geniculate Nucleus. J. Neurosci. *35*, 9265–9280.

Du, J., Blanche, T.J., Harrison, R.R., Lester, H.A., and Masmanidis, S.C. (2011). Multiplexed, high density electrophysiology with nanofabricated neural probes. PLoS One *6*, e26204.

Durand, S., Iyer, R., Mizuseki, K., de Vries, S., Mihalas, S., and Reid, R.C. (2016). A comparison of visual response properties in the lateral geniculate nucleus and primary visual cortex of awake and anesthetized mice. J. Neurosci. *36*, 12144–12156.

Erisken, S., Vaiceliunaite, A., Jurjut, O., Fiorini, M., Katzner, S., and Busse, L. (2014). Effects of locomotion extend throughout the mouse early visual system. Curr. Biol. *24*, 2899–2907.

Evangelio, M., García-Amado, M., and Clascá, F. (2018). Thalamocortical projection neuron and interneuron numbers in the visual thalamic nuclei of the adult C57BL/6 mouse. Front. Neuroanat. *12*, 27.
Gong, S., Doughty, M., Harbaugh, C.R., Cummins, A., Hatten, M.E., Heintz, N., and Gerfen, C.R. (2007). Targeting Cre recombinase to specific neuron populations with bacterial artificial chromosome constructs. J. Neurosci. *27*, 9817–9823.
Granseth, B. (2004). Dynamic properties of corticogeniculate excitatory transmission in the rat dorsal lateral geniculate nucleus in vitro. J. Physiol. (Lond.) *556*, 135–146.
Groh, A., Meyer, H.S., Schmidt, E.F., Heintz, N., Sakmann, B., and Krieger, P. (2010). Cell-type specific properties of pyramidal neurons in neocortex underlying a layout that is modifiable depending on the cortical area. Cereb. Cortex *20*, 826–836.
Guillery, R.W. (1995). Anatomical evidence concerning the role of the thalamus in corticocortical communication: a brief review. J. Anat. *187 (Pt 3)*, 583–592.
Guo, W., Clause, A.R., Barth-Maron, A., and Polley, D.B. (2017). A Corticothalamic Circuit for Dynamic Switching between Feature Detection and Discrimination. Neuron *95*, 180–194.e5.
Hass, C.A., and Glickfeld, L.L. (2016). High-fidelity optical excitation of cortico-cortical projections at physiological frequencies. J. Neurophysiol. *116*, 2056–2066.
Hasse, J.M., and Briggs, F. (2017). Corticogeniculate feedback sharpens the temporal precision and spatial resolution of visual signals in the ferret. Proc. Natl. Acad. Sci. USA *114*, E6222–E6230.
Hoerder-Suabedissen, A., Hayashi, S., Upton, L., Nolan, Z., Casas-Torremocha, D., Grant, E., Viswanathan, S., Kanold, P.O., Clasca, F., Kim, Y., et al. (2018). Subset of cortical layer 6b neurons selectively innervates higher order thalamic nuclei in mice. Cereb. Cortex *28*, 1882–1897.
Jaramillo, J., Mejias, J.F., and Wang, X.-J. (2019). Engagement of Pulvino-cortical Feedforward and Feedback Pathways in Cognitive Computations. Neuron *101*, 321–336.e9.
Jones, E.G. (1985). The Thalamus (New York: Plenum Press).
Li, J., Wang, S., and Bickford, M.E. (2003a). Comparison of the ultrastructure of cortical and retinal terminals in the rat dorsal lateral geniculate and lateral posterior nuclei. J. Comp. Neurol. *460*, 394–409.
Li, J., Guido, W., and Bickford, M.E. (2003b). Two distinct types of corticothalamic EPSPs and their contribution to short-term synaptic plasticity. J. Neurophysiol. *90*, 3429–3440.
Lindström, S., and Wróbel, A. (1990). Frequency dependent corticofugal excitation of principal cells in the cat's dorsal lateral geniculate nucleus. Exp. Brain Res. *79*, 313–318.
Marshel, J.H., Garrett, M.E., Nauhaus, I., and Callaway, E.M. (2011). Functional specialization of seven mouse visual cortical areas. Neuron *72*, 1040–1054.
Mattis, J., Tye, K.M., Ferenczi, E.A., Ramakrishnan, C., O'Shea, D.J., Prakash, R., Gunaydin, L.A., Hyun, M., Fenno, L.E., Gradinaru, V., et al. (2011). Principles for applying optogenetic tools derived from direct comparative analysis of microbial opsins. Nat. Methods *9*, 159–172.
Mease, R.A., Krieger, P., and Groh, A. (2014). Cortical control of adaptation and sensory relay mode in the thalamus. Proc. Natl. Acad. Sci. USA *111*, 6798–6803.

Niell, C.M., and Stryker, M.P. (2010). Modulation of visual responses by behavioral state in mouse visual cortex. Neuron *65*, 472–479.
Olsen, S.R., Bortone, D.S., Adesnik, H., and Scanziani, M. (2012). Gain control by layer six in cortical circuits of vision. Nature *483*, 47–52.
Pachitariu, M., Steinmetz, N., Kadir, S., Carandini, M., and Harris, K.D. (2016). Kilosort: realtime spike-sorting for extracellular electrophysiology with hundreds of channels. BioRxiv.
Pettersen, K.H., Devor, A., Ulbert, I., Dale, A.M., and Einevoll, G.T. (2006). Current-source density estimation based on inversion of electrostatic forward solution: effects of finite extent of neuronal activity and conductivity discontinuities. J. Neurosci. Methods *154*, 116–133.
Przybyszewski, A.W., Gaska, J.P., Foote, W., and Pollen, D.A. (2000). Striate cortex increases contrast gain of macaque LGN neurons. Vis Neurosci *17*, 485–494.
Reichova, I., and Sherman, S.M. (2004). Somatosensory corticothalamic projections: distinguishing drivers from modulators. J. Neurophysiol. *92*, 2185–2197.
Rossant, C., Kadir, S.N., Goodman, D.F.M., Schulman, J., Hunter, M.L.D., Saleem, A.B., Grosmark, A., Belluscio, M., Denfield, G.H., Ecker, A.S., et al. (2016). Spike sorting for large, dense electrode arrays. Nat. Neurosci. *19*, 634–641.
Roth, M.M., Dahmen, J.C., Muir, D.R., Imhof, F., Martini, F.J., and Hofer, S.B. (2016). Thalamic nuclei convey diverse contextual information to layer 1 of visual cortex. Nat. Neurosci. *19*, 299–307.
Schmitzer-Torbert, N., Jackson, J., Henze, D., Harris, K., and Redish, A.D. (2005). Quantitative measures of cluster quality for use in extracellular recordings. Neuroscience *131*, 1–11.
Sherman, S.M. (2016). Thalamus plays a central role in ongoing cortical functioning. Nat. Neurosci. *19*, 533–541.
Sherman, S.M., and Guillery, R.W. (1998). On the actions that one nerve cell can have on another: distinguishing “drivers” from “modulators”. Proc. Natl. Acad. Sci. USA *95*, 7121–7126.
Shobe, J.L., Claar, L.D., Parhami, S., Bakhurin, K.I., and Masmanidis, S.C. (2015). Brain activity mapping at multiple scales with silicon microprobes containing 1,024 electrodes. J. Neurophysiol. *114*, 2043–2052.
Siegle, J.H., López, A.C., Patel, Y.A., Abramov, K., Ohayon, S., and Voigts, J. (2017). Open Ephys: an open-source, plugin-based platform for multichannel electrophysiology. J. Neural Eng. *14*, 045003.
Tsumoto, T., Creutzfeldt, O.D., and Legéndy, C.R. (1978). Functional organization of the corticofugal system from visual cortex to lateral geniculate nucleus in the cat (with an appendix on geniculo-cortical mono-synaptic connections). Exp. Brain Res. *32*, 345–364.
Vélez-Fort, M., Rousseau, C.V., Niedworok, C.J., Wickersham, I.R., Rancz, E.A., Brown, A.P.Y., Strom, M., and Margrie, T.W. (2014). The stimulus selectivity and connectivity of layer six principal cells reveals cortical microcircuits underlying visual processing. Neuron *83*, 1431–1443.
Wang, W., Jones, H.E., Andolina, I.M., Salt, T.E., and Sillito, A.M. (2006). Functional alignment of feedback effects from visual cortex to thalamus. Nat. Neurosci. *9*, 1330–1336.

Wang, W., Andolina, I.M., Lu, Y., Jones, H.E., and Sillito, A.M. (2018). Focal gain control of thalamic visual receptive fields by layer 6 corticothalamic feedback. Cereb. Cortex *28*, 267–280.
Zhou, N.A., Maire, P.S., Masterson, S.P., and Bickford, M.E. (2017). The mouse pulvinar nucleus: Organization of the tectorecipient zones. Vis Neurosci *34*, E011.